A Novel Planar Magnetic Flux Concentrator and Its Application in Wireless Power Transfer

Author

Lu, J, Li, X

Published

2023

Conference Title

2023 IEEE International Magnetic Conference (INTERMAG)

Version

Accepted Manuscript (AM)

DOI

10.1109/INTERMAG50591.2023.10265057

A Novel Planar Magnetic Flux Concentrator and Its Application in Wireless Power Transfer

Junwei Lu[1], *Senior Member, IEEE*, and Xiaokun Li[1], *Student Member, IEEE*

[1]School of Engineering and Built Environment, Griffith University, Nathan, Queensland 4111, Australia

This paper presents a planar magnetic flux concentrator (MFC) to reduce the leakage flux and increase the power transmission in the wireless power transfer (WPT) system. The magnetic field distribution in WPT and eddy current distribution in MFC are investigated. The Finite Element Method (FEM) based simulation results show that the magnetic flux density is increased around the centre hole area of the Tx and Rx coils and decreased in the outer area of the Tx and Rx coils. The experiment results demonstrate that the power transfer can be increased using a planar MFC in the WPT system. The equivalent circuits of WPT transformers with and without a planar MFC are also proposed based on the impedance measurement and analysis. The developed equivalent circuits for the Tx and Rx coils of WPT with MFC are proposed based on the impedance analysis.

***Index Terms*— Magnetic field distribution, magnetic flux concentrator (MFC), FEM, wireless power transfer (WPT).**

I. Introduction

WIRELESS power transfer (WPT) has many advantages, such as safety, convenience, and reliability. There is no risk of electrical sparks or mechanical wear because of the non-contact inherent characteristics, and it can work in extreme environments such as high temperatures and high humidity. WPT has been widely used in smartphones [1], [2], implantable medical devices [3], electric vehicles (EVs) [4]-[6] and unmanned aerial vehicles (UAVs) [7], [8]. However, because WPT uses electromagnetic fields to transfer power, there will be a large leakage magnetic field around the air gap. The leakage magnetic field will reduce power transfer and cause serious EMC/EMI problems in the electronic devices and chips near WPT systems [9].

Much research has been carried out to reduce the leakage magnetic field generated by the transmitting (Tx) and receiving (Rx) coils. Ferrite is a common soft magnetic material used to enhance the magnetic field and reduce leakage magnetic field for improving power transfer [10]. However, this approach leads to an increase in cost and weight. Paper [11] proposed a resonant reactive shield that uses a double-shield coil and phase-shift circuit to reduce magnetic field leakage for EVs wireless charging. This method can effectively reduce the leakage magnetic field. However, it requires two additional coils and four capacitors, which increases system complexity and cost. An optimized core structure for double D coils is proposed to improve the coupling coefficient and power efficiency. The coupling coefficient increases by 30% and effectively improves power transfer efficiency [12]. Tripolar Pad coupling coils are also used to enhance the magnetic coupling to improve the power transfer and can maintain low leakage magnetic flux [13]. However, these methods make the coils' structure more complicated and need more magnetic cores.

The concept of the magnetic flux concentrator (MFC) and its applications have been developed to generate a high AC magnetic field in the past [14]. These devices are very efficient in concentrating the AC magnetic flux and obtaining a high magnetic field. However, the MFC has not been used in WPT systems. Based on the above research, a planar MFC is proposed for use in WPT systems to enhance the useful magnetic field, reduce the leakage magnetic field, and increase power transmission. This MFC does not need extra inductors or capacitors, using only a double-sided PCB, mounted on the opposite side to the transmission (Tx) coil, so the cost is reduced and there is no need to consider the impedance match. In addition, the short-circuited MFC can be used as a traditional passive conducting plate, which can achieve magnetic shielding performance in the WPT system to protect receivers, such as a pacemaker.

In this paper, the electromagnetic simulation models were built to investigate the magnetic field and current distributions, power transfer, and impedance in the case of the Tx coil with and without an MFC. The new equivalent circuit for the Tx and Rx coils with an MFC is proposed based on the impedance analysis. Finally, an experimental platform was built to verify the WPT system.

II. Integration of WPT System with A Planar Magnetic Flux Concentrator

Figure 1 shows the block diagram of the proposed WPT system with a planar MFC. A square wave voltage is generated by the full-bridge inverter which consists of four SiC MOSFETs that can achieve higher power efficiency. To maximize the power transfer from the Tx coil to the Rx coil, two resonant compensation networks (which are usually composed of capacitors and inductors) were added to the T_X coil and Rx coils to achieve impedance matching. The planar MFC is used in the WPT system to concentrate the magnetic field and reduce leakage magnetic flux.

Manuscript received June 8, 2023; (Dates will be inserted by IEEE; “published” is the date the accepted preprint is posted on IEEE Xplore®; “current version” is the date the typeset version is posted on Xplore®). Corresponding author: J. Lu. (e-mail: j.lu@griffith.edu.au).

Color versions of one or more of the figures in this paper are available online at http://ieeexplore.ieee.org.

Digital Object Identifier (inserted by IEEE).

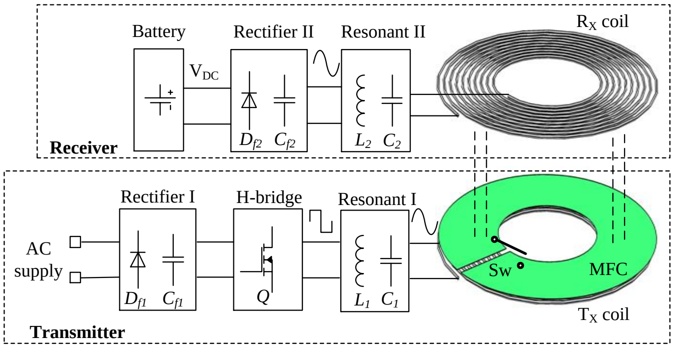

Fig. 1. WPT system diagram using a planar MFC.

This planar MFC is a conductive metal plate with a centre hole and a slit in the radial direction. The MFC is located on the top of Tx coil, and they are stacked together. The switch (**Sw**) is connected to both sides of the slit. The MFC can achieve magnetic field concentration or magnetic shielding when the switch is off or on, respectively. To achieve a perfect electromagnetic performance and considering the manufacture cost, this paper will use copper as the material of the MFC.

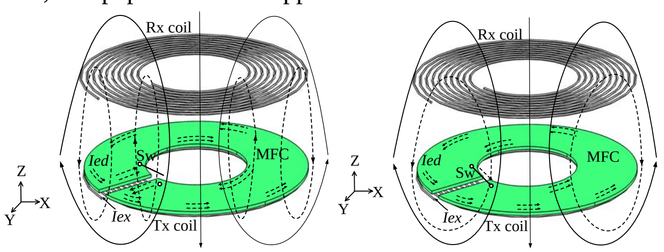

Fig. 2. (a) Magnetic field concentration of the planar MFC, (b) Magnetic shielding by a short-circuited MFC.

Figure 2 (a) illustrates the working principle of magnetic field concentration when the **Sw** of the MFC is off. The solid line indicates the excitation flux lines and the dotted line represents the flux lines generated by the MFC. The Tx coil is spiral-shaped for the exciting current (*Iex*). An assuming current direction is indicated by the arrows for the Tx coil. The opposite direction induction eddy current (*Ied*) is generated on the outward surface of the MFC. The current on the outer surface is conducted inward through the slit, and the current direction on the inner surface of the centre hole is opposite. It then returns to the outer surface through the slit. This effect causes the current around the centre hole to flow in the same direction as the excitation current of the Tx coil, which can generate a magnetic field in the same direction as the magnetic field of the Tx coil. As a result, it can concentrate the magnetic flux and increase the magnetic field strength around the centre hole. Meanwhile, the outer surface current of the MFC flows in the opposite direction as the excitation current. This can offset the magnetic field generated by the Tx coil and reduce the leakage magnetic field. High magnetic flux (φ) will generate a high voltage (e), which is given by

$$e = N\frac{d\varphi}{dt} \tag{1}$$

In addition, if unwanted devices with inner coils are near the receiving side, the slit of the MFC can be short-circuited when the **Sw** is on. The MFC is used as a conducting plate can achieve magnetic shielding by the eddy current (*Ied*). As shown in Fig. 2 (b), the solid line indicates the excitation flux lines, and the dotted line represents the opposite direction of flux lines generated by the MFC that can offset the magnetic field generated by the Tx coil. When an alternating magnetic field is applied to the conducting plate (short-circuited MFC), the relative Maxwell equations are as follows [16]:

$$-\frac{1}{\mu\sigma}\nabla^2\boldsymbol{B} + \frac{\partial \boldsymbol{B}}{\partial t} = 0 \tag{2}$$

Here, $\boldsymbol{B}$ is the magnetic flux, μ and σ are the permeability in vacuum and the conductivity of the conductor plate.

The flux density $\boldsymbol{B}$ can be obtained by using a vector formulation.

$$\boldsymbol{B} = \boldsymbol{B}_m e^{jwt} \tag{3}$$

Here, w is the angular frequency.

Then the flowing equation can be obtained.

$$\nabla^2\boldsymbol{B}_m = jw\mu\sigma\boldsymbol{B}_m \tag{4}$$

If the ideal approximation $w\mu\sigma$=∞ is used, in order that the left-hand term representing the divergence be finite, the following equation must be satisfied.

$$\boldsymbol{B}_m(x, y, z) = 0 \tag{5}$$

Thus, the conducting plate (short-circuited MFC) can achieve magnetic shielding. This phenomenon is caused by the magnetic shielding of conducting plates.

Even though the Rx coil can receive little power due to the leakage flux of the centre hole, it can still achieve a perfect protection function. For example, when some pedestrians with pacemakers or electrical devices approach the Tx coil, they will hardly be affected by the leakage magnetic field which is produced by the Tx coil.

III. Analysis of Magnetic Field Concentration

A. Magnetic Field Concentration

To explain the working principle of the MFC, the Tx coil is excited with a 50 V, 100 kHz sine wave, and the Rx coil is without load. The Z-axis displacement (Zdis) between the Tx and Rx coils is 10 mm. 3D and 2D FEM simulation models are employed to investigate the characteristics of the MFC.

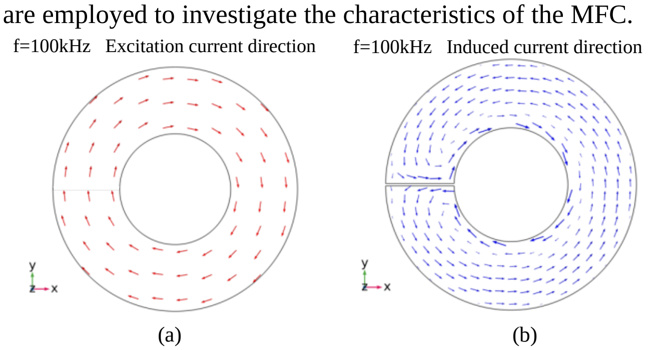

Fig. 3. The current distribution of the Tx coil with the MFC at 10 mm Zdis. (a) excitation current in the Tx coil. (b) eddy current in the MFC.

The current distribution of the Tx coil and the MFC is shown in Fig. 3. Fig. 3 (a) shows the excitation current direction of the Tx coil. From Fig. 3 (b), it can be seen that the induced outer surface current of the MFC flows in the opposite direction as the excitation current of the Tx coil. The current around the centre hole flows in the same direction as the Tx coil excitation current (due to the radial slit). These effects can increase the magnetic flux density around the centre hole and reduce magnetic flux density around the outside area of the Tx coil.

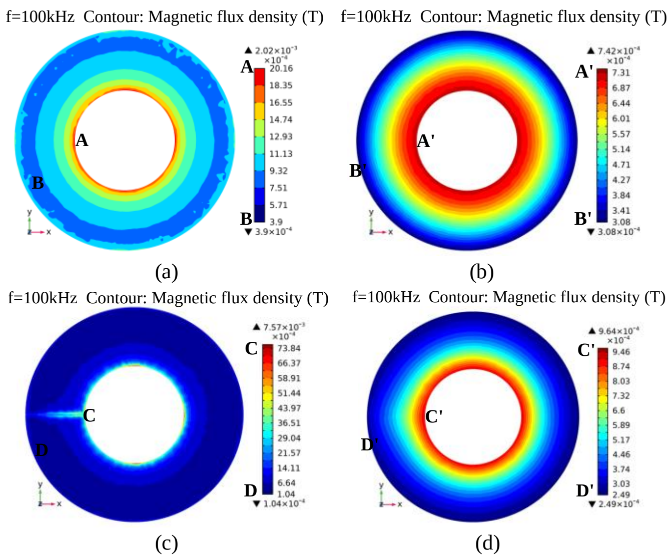

Fig. 4. The magnetic flux density at 10 mm Zdis. (a) Tx coil (Tx without an MFC). (b) Rx coil (Tx without an MFC). (c) Tx coil (Tx with an MFC). (d) Rx coil (Tx with an MFC)

Figure 4 (a), (b) show the magnetic field distribution in the case of the Tx coil without an MFC. The maximum and minimum contour areas for the magnetic flux densities of the Tx and Rx coils are noted as '**A**', '**B**' and '**A'**', '**B'**', respectively. They are 2.02×10^{-3} T, 3.9×10^{-4} T, and 7.42×10^{-4} T, 3.08×10^{-4} T, respectively. Fig. 4 (c), (d) show the magnetic field distribution in the case of the Tx coil with an MFC. The maximum and minimum contour areas for the magnetic flux densities of the Tx and Rx coils are noted as '**C**', '**D**' and '**C'**', '**D'**', respectively. They are 7.57×10^{-3} T, 1.04×10^{-4} T, and 9.64×10^{-4} T, 2.49×10^{-4} T, respectively. Compared with Fig. 4 (a) and (c), in the case of the Tx coil with an MFC, the flux density around the centre hole of the Tx coil is increased by 274.75% and flux density around the outer surface is reduced by 73.33%. Meanwhile, in the case of the Tx coil with an MFC, the flux density around the centre hole of the Rx coil is increased by 29.92%, reduced by 19.16% around the outer surface, when compared with Fig. 4 (b) and (d). These results prove that using the MFC can reduce the leakage magnetic field around the outer surface and increase magnetic flux density around the centre hole of the Tx and Rx coils.

B. Magnetic Flux Concentrator with Different Thickness

The slit width and thickness of the MFC were investigated for optimizing the MFC design. The Tx coil is excited with a 50 V, 100 kHz sine wave, and the Rx coil is without load. The Z-axis displacement (Zdis) is 10 mm. Fig. 5 shows the mean flux density of the coils and voltage of the R_X coil under different thicknesses of the MFC. With an increased thickness of the MFC, the mean flux density of the T_X and R_X coils increased. It leads to an increased receiving voltage (R_X voltage) slightly at the fix distance (10 mm). It shows that the design of the MFC should have a higher thickness.

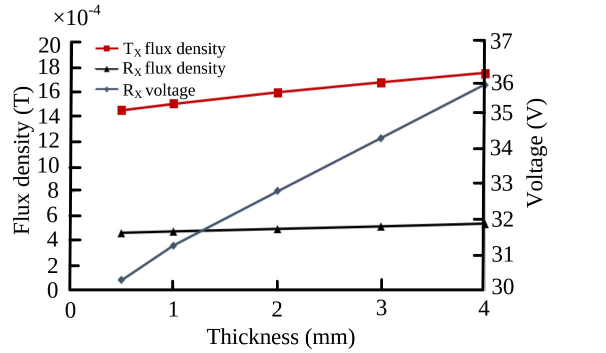

Fig. 5. Flux density and voltage of the R_X coil variation with the thickness of the MFC at 10 mm Zdis.

C. Magnetic Shielding by A Short-circuited MFC

The magnetic shielding effect can be obtained when the slit of the MFC is short-circuited (the switch (**Sw**) is on). At this time, the short-circuited MFC is a conducting plate. Fig. 6 shows the flux lines in the case of the T_X coil without an MFC and with a short-circuited MFC at 10 mm Zdis. From Fig. 6 (b), most of the flux lines are shielded by the short-circuited MFC. The flux lines crossed by the R_X coil are greatly reduced.

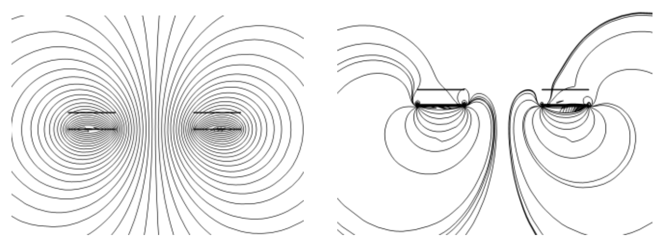

(a) (b)

Fig. 6. Flux lines at 10 mm Zdis. (a) T_X coil without the MFC. (b) T_X coil with a short-circuited MFC.

With an increased Zdis, the magnetic flux and voltage of the R_X coil are reduced. In the case of the T_X coil with a short-circuited MFC, the magnetic flux of the R_X coil is very small, and the voltage of the R_X coil is less than 2.25 V. It can achieve perfect magnetic shielding to protect the receiving side.

IV. EQUIVALENT CIRCUIT OF WPT WITH MFC

A test platform was built to test the impedance and verify the accuracy of the simulation results. The printed circuit board (PCB) coils are used as the T_X and R_X coils which are shown in Fig. 7 (a).

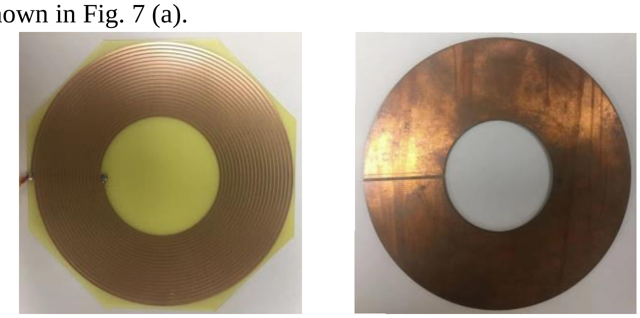

(a) (b)

Fig. 7. The test platform of the T_X and R_X coils and MFC. (a) T_X and R_X coils. (b) the MFC.

A. Impedance Measurement from Test and Simulation

TABLE I. RESULTS OF T_X COIL SIMULATION CALCULATION AND TEST.

	Inductance without an MFC	Inductance with an MFC	Resistance without an MFC	Resistance with an MFC
Test	37.05 μH	30.562 μH	3.305 Ω	4.591 Ω
Simulation	37.165 μH	31.84 μH	2.26 Ω	4.147 Ω
Calculation	37.682 μH			

The MFC is made up of a planar PCB copper plate with a centre hole and a radial direction slit, which is shown in Fig. 7 (b). Their parameters are listed in Table I, it should be noted that the thickness of copper is 37.5 μm for the coils and MFC in this section. To ensure the correctness of simulation parameters and models, the self-inductance and resistance of the T_X coil with and without an MFC were simulated and compared with theoretical calculation and experimental testing. The results are shown in Table I.

The calculated inductance of the Tx coil without an MFC can be obtained by the following equation [23].

$$L = \mu n^2 d_{avg} c_1 / 2(\ln(c_2/\rho) + c_3\rho + c_4\rho^2) \tag{6}$$

Here, the outer diameter is d_{out}, the inner diameter is d_{in}, the average diameter is d_{avg}=0.5(d_{out}+d_{in}), the fill ratio is defined as ρ=(d_{out}-d_{in})/(d_{out}+d_{in}), and the c_1, c_2, c_3, c_4 are 1.00, 2.46, 0, and 0.20, respectively.

From Table I, it is evident that the test, simulation, and calculation of the inductances and resistances are very close, which can prove that the parameters and the model of as the simulation are correct.

Open-circuit testing is carried out to investigate the magnetizing resistance and magnetizing inductance. The R_X coil is open-circuited, and the T_X coil is connected to the LCR meter.

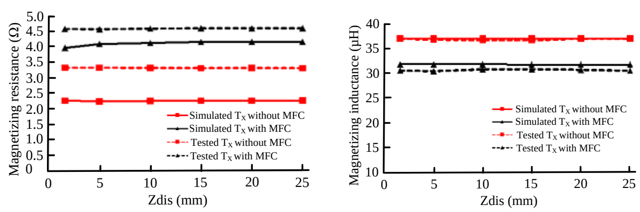

(a) (b)

Fig. 8. Magnetizing impedance variation with the Zdis. (a) magnetizing resistance (R_C). (b) magnetizing inductance (L_m).

Figure 9 shows the simulated and tested results of magnetizing resistance (R_C) and magnetizing inductance (L_m) variation with Zdis in the case of the T_X coil with and without an MFC. As shown in Fig. 9 (a), The testing R_C in the case of the T_X coil with and without an MFC is about 4.592 Ω and 3.305 Ω, respectively. It can be seen that adding an MFC to the T_X coil increases the R_C. As shown in Fig. 9 (b), the testing L_m in the case of the T_X coil with and without an MFC is about 30.873 μH and 37.055 μH, respectively, which shows that adding an MFC to the T_X coil reduces the L_m. The same results can be obtained for X_m because X_m is proportional to L_m. The testing results agreed with the simulation results. There are some errors between the simulation and testing results because the simulation parameters are ideal, and the cables of the LCR will affect the measurement results. In addition, the copper oxide on the surface of the copper wire and two short wires connected to coil terminals for testing will also lead to measurement errors.

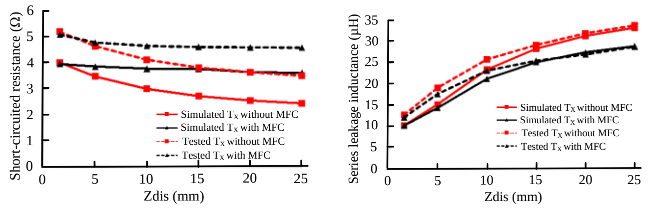

(a) (b)

Fig. 9. Short-circuited impedance variation with the Zdis. (a) short-circuited resistance (R_1+R_2'). (b). leakage inductance (L_{l1}+L_{l2}').

Short-circuit testing was used to obtain the equivalent series short-circuited resistance and equivalent series leakage inductance. The Rx coil is short-circuited and the Tx coil was connected to the LCR meter.

The equivalent series short-circuited resistance (R_1+R_2') and leakage inductance (L_{l1}+L_{l2}') variation with the Zdis under different scenarios (Tx coil with and without the MFC) are shown in Fig. 10. As shown in Fig. 10 (a), the short-circuited resistance (R_1+R_2') is reduced with the increased Zdis. However, the short-circuited resistance (R_1+R_2') is higher in the case of the T_X coil with an MFC than the T_X coil without an MFC. As shown in Fig. 10 (b), with the increased Zdis, the series leakage inductance (L_{l1}+L_{l2}') is increased due to poor magnetic coupling. However, compared with the condition that did not use an MFC, the tested series leakage inductance reduces by 17.56% when using an MFC at a 25 mm Zdis. The leakage magnetic field was also effectively reduced. With the increment of the air gap, using the MFC can result in more reduction in the leakage inductance. The same results can be obtained for X_{l1} and X_{l2}' because they are proportional to L_{l1} and L_{l2}'.

B. Proposed Equivalent Circuit

An LCR meter is used to investigate the resistance and inductance to obtain an equivalent circuit for the Tx and Rx coils with and without an MFC.

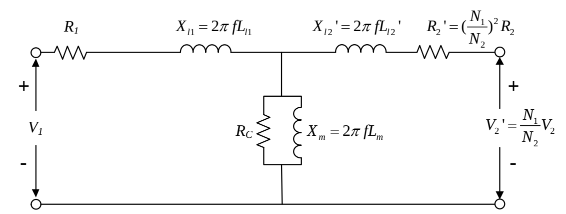

(a)

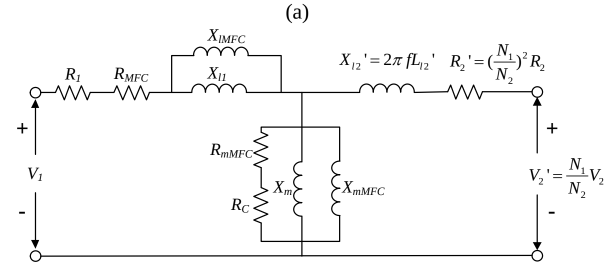

(b)

Fig. 10. Equivalent circuit, (a) T_X coil without an MFC, (b) T_X coil with an MFC.

Figure 8 (a) shows the equivalent circuit for the Tx and Rx coils in the case of the Tx coil without an MFC, which is shown as a traditional transformer. V_1, R_1, X_{l1}, and L_{l1} are the voltage, resistance, leakage inductance reactance, and leakage inductance of the T_X side. R_C is magnetizing resistance. X_m and L_m are magnetizing inductance reactance and magnetizing inductance. V_2 and R_2 are the voltage and resistance of the R_X side; V_2' and R_2' are the values that the R_X side referred to the T_X side. X_{l2}' and L_{l2}' are the leakage inductance reactance and leakage inductance that the R_X side referred to the T_X side. N_1 and N_2 are the turns of the T_X and R_X coils, and both of them are the same (n=20). f is excitation frequency.

Figure 8 (b) shows the equivalent circuit for the Tx and Rx coils in the case of the Tx coil with an MFC. R_{MFC} is in series to the circuit indicating the increment of the series short-circuited resistance. X_{lMFC} is parallel to the X_{l1} indicating the decrease of the equivalent series leakage inductance reactance. R_{mMFC} is in series to R_C indicating the increment of the magnetizing resistance. X_{mMFC} is parallel to X_m indicating the decrease of the magnetizing inductance reactance. The detailed impedance change is introduced in the following open-circuit and short-circuited impedance analysis.

C. Voltage Ratio Measurement

A 10 V, 100 kHz sine wave source is used to test the open-loop voltage ratio and waveforms of the T_X and R_X coils.

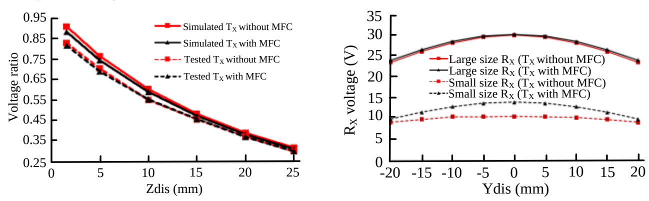

(a) (b)

Fig. 11. (a) open-loop voltage ratio of two coils variation with the Zdis, (b) voltage variation with the Ydis using different RX coils at 10 mm Zdis.

Figure 10 (a) shows the simulated and tested open-loop voltage ratio of the T_X and R_X coil variation with the Zdis under different scenarios (T_X with and without an MFC). It can be seen that the voltage ratios were reduced with the increase of the Zdis. When the Zdis is 1.6 mm (because of the thickness of the MFC), the voltage ratios are maximum because of the perfect coupling. The voltage ratios are almost the same regardless of whether the Tx coil is with or without an MFC under the same Zdis, which is consistent with the former analysis. The testing voltage ratio is smaller than the simulated voltage ratio mainly because the copper oxide on the surface of the copper wire will lead to more voltage drop. Fig. 10 (b) shows the voltage of the Rx coil variation with Y-axis displacement (Ydis) using the large size and small size Rx coil at 10 mm Zdis. These results indicated that more magnetic flux could be concentrated in the Rx coil which resulted in higher induced voltage at the terminal of the Rx coil for the small Rx coil size. Therefore, more power can be transferred from the Tx coil to Rx coil.

V. Conclusion

This paper proposed a planar MFC used in the WPT system for the magnetic field concentration and reducing the leakage magnetic field and increasing power transfer. The electromagnetic field simulation and experimental testing were carried out to investigate the magnetic field, power transfer, and impedance of WPT coils with MFC.

The results indicated that the T_X coil using a planar MFC could increase the magnetic flux density of the T_X and R_X coils around the centre hole, and reduce the magnetic flux density on the outer surface of the T_X and R_X coils, and the leakage magnetic field. When the MFC was short-circuited, perfect magnetic shielding could be achieved. The investigation also discovered that the MFC to the T_X coil could increase the voltage and power of receiving coil (R_X) in the case of a small-size R_X coil. The equivalent circuit of the T_X and R_X coils with an MFC has been obtained based on the analysis of the impedance of WPT coils.

References

[1] J. Zhu, Y. Ban, Y. Zhang, Z. Yan, R. Xu and C. C. Mi, "Three-coil wireless charging system for metal-cover smartphone applications," *IEEE Trans. on Power Electron.*, vol. 35, no. 5, pp. 4847-4858, May 2020.

[2] W. Xu, W. Liang, J. Peng, Y. Liu and Y. Wang, "Maximizing charging satisfaction of smartphone users via wireless energy transfer," *IEEE Trans. on Mobile Comput.*, vol. 16, no. 4, pp. 990-1004, 1 April 2017.

[3] C. Liu, C. Jiang, J. Song and K. T. Chau, "An effective sandwiched wireless power transfer system for charging implantable cardiac pacemaker," *IEEE Trans. on Ind. Electron.*, vol. 66, no. 5, pp. 4108-4117, May 2019.

[4] M. S. A. Chowdhury and X. Liang, "Design and performance evaluation for a new power pad in electric vehicles wireless charging systems," *Can. J. of Elect. and Comput. Eng.*, vol. 43, no. 3, pp. 146-156, Summer 2020.

[5] L. Wu, B. Zhang and J. Zhou, "Efficiency improvement of the parity-time-symmetric wireless power transfer system for electric vehicle charging," *IEEE Trans. on Power Electron.*, vol. 35, no. 11, pp. 12497-12508, Nov. 2020.

[6] A. Zakerian, S. Vaez-Zadeh and A. Babaki, "A dynamic WPT system with high efficiency and high power factor for electric vehicles," *IEEE Trans. on Power Electron.*, vol. 35, no. 7, pp. 6732-6740, July 2020.

[7] M. Lu, M. Bagheri, A. P. James and T. Phung, "Wireless charging techniques for UAVs: a review, reconceptualization, and extension," *IEEE Access*, vol. 6, pp. 29865-29884, 2018.

[8] C. Cai, S. Wu, L. Jiang, Z. Zhang and S. Yang, "A 500-W wireless charging system with lightweight pick-up for unmanned aerial vehicles," *IEEE Trans. on Power Electron.*, vol. 35, no. 8, pp. 7721-7724, Aug. 2020.

[9] S. Kong, B. Bae, D. H. Jung, J. J. Kim, S. Kim, C. Song, J. Kim, J. Kim, “An investigation of electromagnetic radiated emission and interference from multi-coil wireless power transfer systems using resonant magnetic field coupling,” *IEEE Trans. on Microw. Theory and Techn.*, vol. 63, no. 3, pp. 833-846, March 2015.

[10] M. Mohammad, S. Choi and M. E. Elbuluk, "Loss minimization design of ferrite core in a dd-coil-based high-power wireless charging system for electrical vehicle application," *IEEE Trans. on Transp. Electrific.*, vol. 5, no. 4, pp. 957-967, Dec. 2019.

[11] H. Moon, S. Kim, H. H. Park and S. Ahn, "Design of a resonant reactive shield with double coils and a phase shifter for wireless charging of electric vehicles," *IEEE Trans. on Magn.*, vol. 51, no. 3, pp. 1-4, March 2015.

[12] H. Zeng, Z. Liu, Y. Hou, T. Hei and B. Zhou, "Optimization of magnetic core structure for wireless charging coupler," *IEEE Trans. on Magn.*, vol. 53, no. 6, pp. 1-4, June 2017.

[13] S. Kim, G. A. Covic and J. T. Boys, "Tripolar pad for inductive power transfer systems for EV charging," *IEEE Trans. on Power Electron.*, vol. 32, no. 7, pp. 5045-5057, July 2017.

[14] K. Bessho, M. Furuta, M. Hayashigishi, S. Imamura, S. Yamada, and M. Enokizono, “Characteristics of multilayer eddy-current type coil with core,” *IEEE Transl. J. on Magn. in Jpn.*, vol. 6, no. 6, pp. 515-523, June 1991.